ISSN: 0974-5823 Vol. 7 No. 5 May, 2022

International Journal of Mechanical Engineering

Back-to-Back Voltage-Source Converters with ANFIS Controller for Grid-Associated Wind-Solar Cogeneration

MUTHOOJU BHARATH KUMAR[1], M. SRIKAR[2], I. VIJAY KUMAR[2], DR. T. ANIL KUMAR[3]

[1]PG Scholar, Department of Electrical and Electronics Engineering, Anurag Group of Institutions (Anurag University), Venkatapur, Ghatkear, Medchal Malkajgiri District, Telangana, India 500088. E mail-muthoojubharath123@gmail.com

[2]Assistant Professor, Department of Electrical and Electronics Engineering, Anurag University, Venkatapur, Ghatkear, Medchal Malkajgiri District, Telangana, India 500088.

[3]Professor, Department of Electrical and Electronics Engineering, Anurag University, Venkatapur, Ghatkear, Medchal Malkajgiri District, Telangana, India 500088

Abstract: The main aim of this project is Back-to-Back Voltage-Source Converters with Adaptive neuro fuzzy inference (ANFIS) Controller for Grid-associated Solar/Wind Cogeneration to reach the desired performance level. An effective and simple wind-solar cogeneration system has been proposed in this research. Utilizing BtB VSCs with ANFIS controller tuning, a wind turbine is connected to the grid. A dc-link capacitor was used to directly connect a PV generator. There are no phases conversion of DC/DC in this system. In addition, to maximise the extraction of renewable energy, the proposed topology incorporates tracking of the individual maximum power points of PV and Wind generators. An ANFIS controller with vector control in a rotating reference frame is used to control the VSCs. The suggested system's performance is also examined in light of utility-grid issues. MATLAB/SIMULINK findings are used to verify the proposed topology's efficiency.

Key words: Grid, PV, Wind, Back-to-Back voltage-source converters (VSCs), Adaptive neuro fuzzy inference (ANFIS) Controller

I.INTRODUCTION

Over the last decade, the cost of wind and solar power has declined significantly. Renewable energy sources including solar and wind have grown from a total of six gigawatts in 2006 to more than 303 gigawatts in 2016 because of economic and technical incentives [1]. Distributed generating units are built using power-electronic converters since wind and solar energy is unpredictable and uncontrollable. There is a lot of discussion about distributed generating systems using renewable sources like solar and wind power. Wind and solar power are examples of renewable energy. and solar have recently being studied in tandem. to optimise the advantages of the available renewable resources [9]. When wind and solar energy are combined, the total operating efficiency is increased because of the complimentary nature of t two sources of energy. Due to a smaller footprint of combined scheme, the hybrid solar and wind co-generators maximise land resources usage and hence improve capital investments. Furthermore, wind turbines have a greater capacity to assist the utility grid dynamically than static solar generators because of their mechanical inertia. In the event of an outage, you'll have a backup supply of power. Unfortunately, grid-tied wind and solar cogeneration generators get less attention in the literature. Wind and solar hybrid systems, on the other hand, may be used to power off-grid homes and businesses. [10]. In grid-connected and stand-alone applications, proposes an optimum sizing technique for wind-solar-battery systems. Multiple-input converters were used to enhance the integration of renewable energy sources in [12]– [14]. For example, in [12], it is suggested to fuse two types of DC-DC converters together. In [13] and [14], a current-source dc-dc converter and a linked transformer are both presented. Aside from complicated topologies, the suggested Dc power distribution may not be the best medium for ac-dominated power systems [12]. In light of this, the technologies detailed here have not been put to the test in higher-power

applications. In a freestanding hybrid solar and wind arrangement includes diesel engines and battery storage. Multiple converters linked in parallel to interconnected renewable energy resources are commonly connected via a single DC bus, which may reduce overall system efficiency and increase overall system costs. Because of this, controller design and coordination are essential to minimise the dynamic interactions between the closely regulated converters of energy An unstable system could be introduced by using power converters. Electricity is supplied to the PV generator and energy storage unit through dc-dc converter-interfaced VSCs. Wind-powered induction generator is connected to a battery bank through a VSC, which is subsequently charged by a PV generator. RES such as wind and the sun need the use of hybrid systems. just a small amount of electrical power throughout the conversion process. These systems, on the other hand, are aimed toward specialised off-grid uses. [15] seems to be the primary source of information on the Grid-associated solar and wind energy systems. The BtB VSC coupling the wind turbines and solar to the electrical grid in [15]. It is possible to control the DC-link voltage based on the MPPT value of the PV panel, using a PI dc voltage controller on the machine side. By using the synchronous detection technique, the machine-side current reference values are identified, and a hysteresis current controller (HCC) is used to regulate them. Despite the fact that [15]'s method has the potential to be beneficial, difficulties must be addressed: Using both VSCs in the MPPT for PV or wind production might impair system reliability and increase losses in certain scenarios. This means that if there is no wind power, then wind turbines may not be able to produce energy. The wind turbine's speed is not controlled by a servo operation. The gadget controls the dc-link voltage. In order to boost the harmonic content of machine and grid side currents, hysteresis controllers are utilised. Hybrid wind-solar producing systems have been touted for their potential benefits, as well as the challenges encountered by the renewable energy sector, which motivated this investigation.

A novel topology for connecting wind and solar generators to the electric grid has been developed, and it is simpler and more efficient than the one described in [15]. What the document has to provide is as follows: The integrated BtB VSCs, which don't need any additional power electronic switches, may be used to realise linked wind and solar power plants to the utility grid An ANFIS controller and a voltage-source rectifier (VSR) are the sole means of achieving maximum power point tracking (MPPT) in utility grids by regulating the dc-link voltage (MPPT). The suggested system's overall stability is characterised using a small-signal state-space model. 4) The hybrid system that has been proposed has performance has been evaluated using time-domain simulations in a number of operational scenarios, including utility-grid outages.

II. PROPOSED SYSTEM

The suggested system is indicated in Figure. 1, the arrangement contains voltage source rectifier to link the wind generator, and voltage source inverter to coupled to the hybrid cogeneration system into the grid. By using a dc cable, the BtB VSCs' dc-link capacitor is directly connected to the PV generator. There are six cells in the VSR and VSI, each of which has an IGBT connected to a diode. In the next segments, the suggested system's modelling and control are detailed.

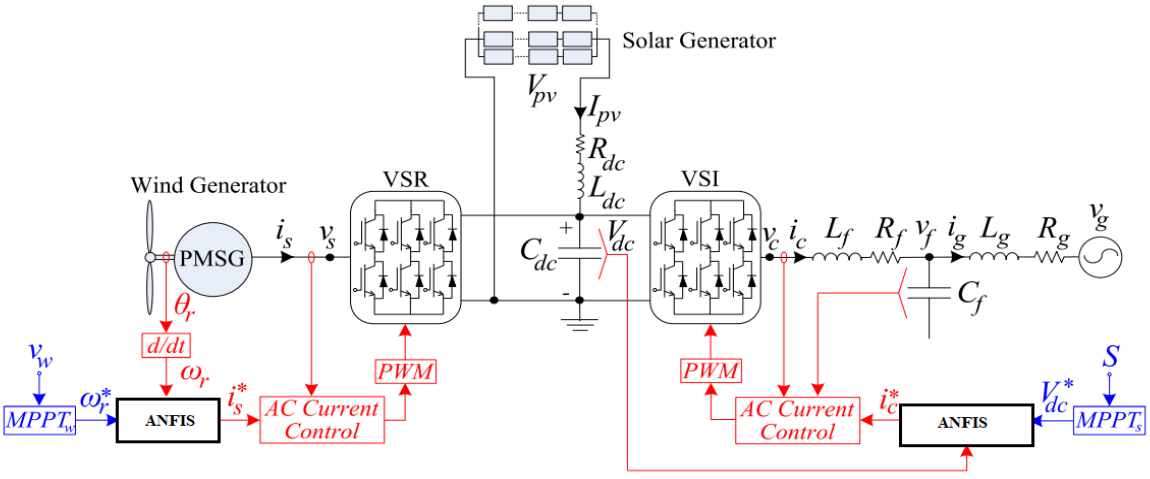

Fig.1 Proposed Grid-Connected Cogeneration of Wind and Solar Energy ANFIS Controller-Controlled BtB VSCs

Wind Generator Modelling

The PMSG is used in a full-scale wind turbine (FSWT) because of its low operational and maintenance costs [2]. According to the wind turbine model, it looks like this:

$$P_m = \frac{1}{2} C_p(\beta, \lambda) \rho \pi R^2 v_{wind}^3, \lambda = \frac{R\omega_r}{v_{wind}} \quad (1)$$

Rotor power coefficient (Cp), which is nonlinearly related to the blade pitch angle and the speed ratio of tip, is defined as a function of Pm and Cp. Normal operational conditions are optimised for wind power generation by setting at zero [13]. In the following way, the PMSG is modelled.

$$\overline{v_s} = R_s \overline{\imath_s} + L_s \frac{di_s}{dt} + jp\omega_r (\psi + L_s \overline{\imath_s}) \quad (2)$$

$$J \frac{d}{dt} \omega_r = \frac{3}{2} p \psi I_{sq} - T_m \quad (3)$$

where $\overline{\imath_s}$ and $\overline{v_s}$ are current and voltage in stator and the representation of complex vectors, correspondingly, Complex vectors xd +jXq are the quadrature and direct apparatuses of the rotating reference frame's complex vector x in the rotating reference frame; Ls is inductance of stator; Rs is stator-winding resistance. A motor's inertia and viscous friction are represented by J and, respectively, the imaginary unit number, the rotor magnet flux linkage, the mechanical rotor speed, and the number of pole pairs in the scheme.

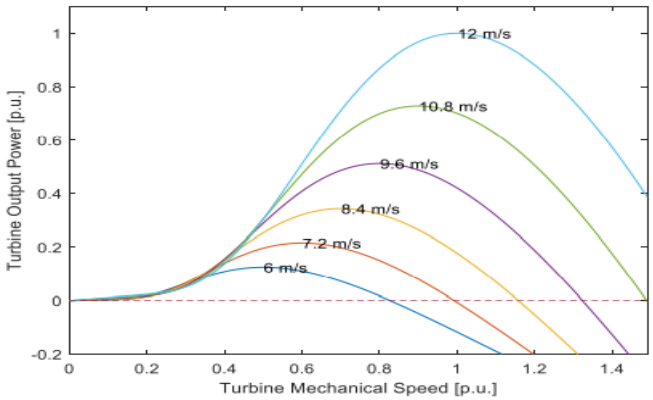

Fig.2. At varying wind speeds, the wind turbine's mechanical properties change.

Wind speed and mechanical rotor speed are displayed in Fig.2 as a function of the produced turbine power. When the rotor speed is perfectly adjusted to match the changing wind speed, the most wind power is created. According to Fig. 1, an MPPT for the wind generator (MPPTw) may be used to provide a reference value for the PMSG rotor rotor speed (r) at the VSR-side.

Machine-Side VSR Modelling

With the help of the Gs(s) controller, which regulates the PMSG mechanical rotor speed in accordance with its MPPTw characteristics, the maximum wind power may be captured (4).

$$I_{sq}^* = (\omega_r^* - \omega_r) G_s(s), I_{sd}^* = 0 \quad (4)$$

To build the ANFIS speed controller, the outer loop is used. The stator current reference (I sq) may operate at its maximum torque, the controller sets its I-component value to zero, as well as its I-component value for the stator current reference (I sd). The speed controller's gps and gis settings, for example, may be adjusted to meet your needs. This controller is in order to guarantee that the PMSG stator currents are controlled by the ANFIS current controller in the inner loop, the ANFIS controller is constructed.

$$\overline{v_s} = \left(\overline{\imath_s^*} - \overline{\imath_s}\right) G_i(s) + jP\omega_r^0 L_s \overline{\imath_s} + jP\psi H\omega_r \quad (5)$$

Note that jPω◦ rLs ¯ signifies the variable's steady-state value. The current controller is constructed in a manner similar to the speed controller's by solving (2) and (5).

Grid-Side Voltage Sources Inverter (VSI) Modelling

Internal resistance in an inductive filter (Lf) terminates the VSI's ac side (Rf). (Cf). 3-phase currents and voltages are shown in the VSI as vc/ic. To represent the three-phase rms utility grid voltage and current as impedance, an inductive component (Lg) is coupled to the equivalent resistance of the line (Rg). The following equations simulate the utility-grid impedance and the Lf Cf filter:

$$\overline{v_c} = \overline{v_f} + R_f\overline{i_c} + L_f\frac{di_c}{dt} + j\omega L_f\overline{i_c} \qquad (6)$$

$$\overline{v_f} = \overline{v_g} + R_g\overline{i_g} + L_g\frac{di_g}{dt} + j\omega L_g\overline{i_g} \qquad (7)$$

$$\overline{i_c} = C_f\frac{d\overline{v_f}}{dt} + \overline{i_g} + j\omega C_f\overline{v_f} \qquad (8)$$

The PLL is utilised to synchronise the converter to the grid in (9), which regulates the VSI.

$$\omega = \omega^0 + \frac{V_{fq}^c}{V_{fd}^c}K_\delta(S) \qquad (9)$$

In (9), (Kδ (s) is Set the PCC voltage (Vcq) to zero and produce synchronisation by using an ANFIS controller in the PLL structure. The dissociating of reactive and active power is a key benefit of vector control. management. Icd can be used to control the VSI's active power injection (Pvsi) but not its reactive power injection (Rpi). (Qvsi) is totally reliant on Icq, as illustrated in (10) (11).

$$P_{vsi} = Real\left\{1.5\overline{v_c}\,\overline{i_c^{conjugate}}\right\} = 1.5V_{cd}I_{cd} \qquad (10)$$

$$Q_{vsi} = Iamginary\left\{1.5\overline{v_c}\,\overline{i_c^{conjugate}}\right\} = 1.5V_{cd}I_{cq} \quad (11)$$

III.ANFIS CONTROLLER

Neuro-fuzzy adaptive inference system is the abbreviation for ANFIS. It is a combination of fuzzy logic and neural network. Many inputs are passed via the neural network, depending on the inputs. The performance and inputs of the neural network are used to train it. After training the neural network, the performance is incorporated to the fuzzy logic. Fuzzy logic generates the rules (IF and THEN) and membership functions (MF). The ANFIS architecture is shown in the figure.4 below.

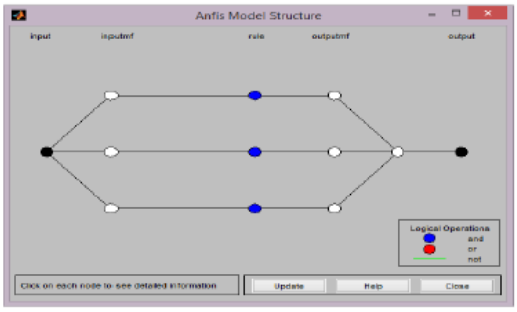

Fig. 3. ANFIS architecture

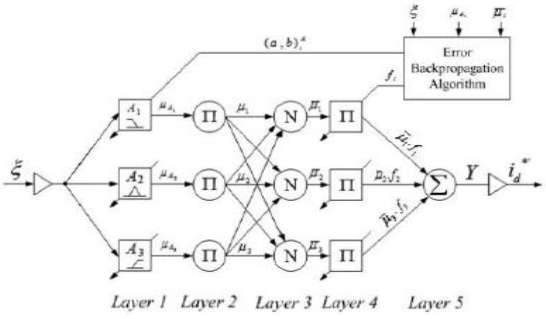

Fig.4 Schematic of the proposed ANFIS

A There will be an inaccuracy in the Neurofuzzy controller when comparing the dc-link reference voltage to the actual DC-link voltage. (ξ = Vdc*-Vdc), A similar mistake will likewise affect the precondition and the subsequent parameters. The active current (id*') component of the dc-link voltage controller is utilized to compute the active current injected into RES (iRen).

Layer 1: This is when things start to become fuzzy. In this layer, each input variable's membership degree is determined. Error (e) and error change (e) are the ANFIS input variables. trapezoidal and triangle registration capabilities are used to decrease measurement error as illustrated in Figure 5.as explained below the node criteria are,

$$O_i^1 = \mu_{Ai}(x) = \frac{1}{1+\left[\left(\frac{x-c_i}{a_i}\right)^2\right]^{bi}} \qquad (12)$$

Premise parameters are defined as follows: x is the node-i entry; Ai is the linguistic variable connected with it; and bi, ci is the premise parameter set.

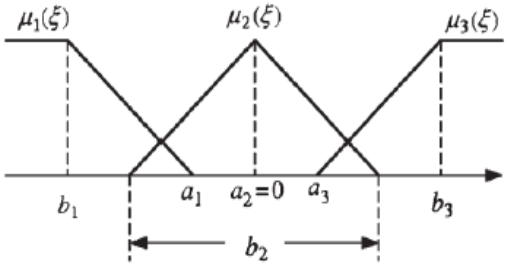

Fig. 5 Fuzzy membership functions.

The second layer of the rule is called the "inferior" layer. In this layer, each node is a fixed node whose input is multiplied and the result is sent out. Using a fuzzy rule, the amount of energy used by each node is represented by its firing strength.

$$O_i^2 = \mu_i = \mu(x)\mu(y) \qquad i = 1,2,3 \qquad (13)$$

Layer 3: The normalising layer is what it sounds like. An N-labeled circular node represents each node in a layer. The i-th node calculates the ratio of the rules' firing force to the total firing force.

$$O_i^3 = \overline{\mu_i} = \frac{\mu_i}{\mu_1+\mu_2+\mu_3} \qquad i = 1,2,3 \qquad (14)$$

Layer 4: It's the final product. Functionality and adaptable mode is available on all nodes.

$$O_i^4 = \overline{\mu_i}.f_i = \overline{\mu_1}(a_0^i + a_1^i\epsilon) \;\; i = 1,2,3 \quad (15)$$

The resulting parameter set where the output of Layer 3 is wi (a0, a1).

Layer 5: As the name implies, here is where the data is sent out to the outside world. In this layer, there is just one node, which is the sum of all the input signals, and it is labelled as.

$$O_i^5 = \mu_i = \sum_i \overline{\mu_i} f_i \qquad i = 1,2,3 \qquad (16)$$

Errors in the back propagation of the ANFIS parameters are corrected.

$$\frac{\partial E}{\partial O^5} = k_1.e + k_2.\Delta e \qquad (17)$$

The k1 and k2 coefficients are multiplied to get the error (e) and the change in error (e).

$$\alpha_{k+1} = \alpha_k - n\frac{\partial E}{\partial \alpha_k} \qquad (18)$$

When a certain ANFIS parameter is used, the study rate is. The mistake will be included into the following round of training

IV. SIMULATION RESULTS

The below figure .6 indicates the MATLAB/SIMULINK circuit diagram of the solar-wind co-generation system.

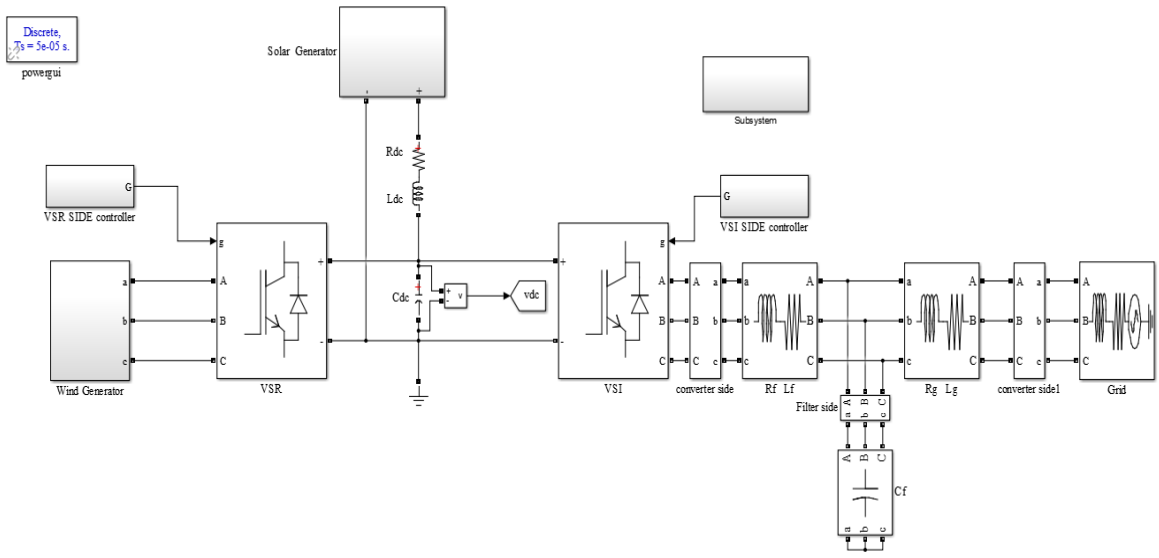

Fig. 6 MATLAB/SIMULINK circuit diagram of the wind-solar cogeneration system

RESULTS WITH PI CONTROLLER

Cogeneration of wind and sun energy is investigated under a variety of meteorological conditions. After two, four, and six seconds, the speed of wind increases from 8.4 to 10.8 metres per second, then decreases to 7.2 metres per second before rising again to 12 metres per second (a). t = 3, 5, and 6 s, correspondingly, the solar irradiance level decreases from one to one with the wind speed changes. The MPPTw and MPPTs in Figures 2 and 3 are used to derive the ideal r and V dc. Figs. 7d and (e), respectively, illustrate the generated wind power and solar power as well as the injected currents into the utility grid as a result of the well-damped performance of r and Vdc 7(f). At night, when irradiation levels are low, a PV generator produces zero (or minimum) power. Figure 8(a) shows the dc-link voltage dropping to 0.858p.u. at t = 2.0 s when the PV power generation drops to zero, and then rising to 1.0p.u. at t = 3.0 s. Figures 8(b) and (c) show wind energy and solar energy, as well as the ac current pumped into the electric grid (c).

According to Fig. 9, at times of t = 2 and 3 seconds, the controller is employed to reduce the r value from 1 psu to 0. (a). This correlates to a dramatic decrease in wind speed from 0 to 1 p.u. as indicated in Fig. 9. (b). It is possible to keep a system stable in a challenging operating environment.

With 1.0 p.u. of wind power generation and solar power generation, the system's performance is shown in Figure 10. Figure 10 illustrates the point. Since then, the grid's ac current injection has been stabilised, although the dc-link voltage has risen.

When a single-phase-to-ground (1PG) failure occurs, the system behaves as shown in Figure 10. Figure 8's 3PG faults clearly have a detrimental influence on system performance, but the 1PG fault has no effect. According to Fig. 11, the dc-link response of the protected system is significantly more damped when compared to that of the unprotected case.

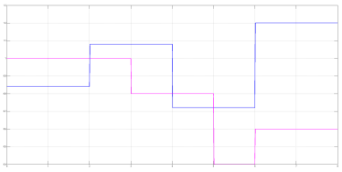

(a) Speed of wind & solar irradiance

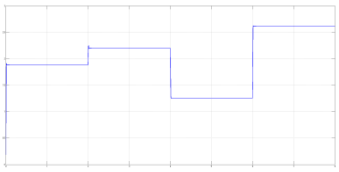

(b) Speed of PMSG

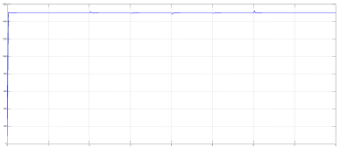

(c) Voltage at the DC link

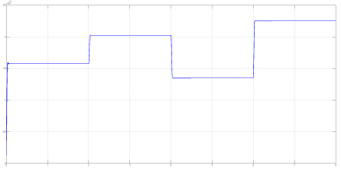

(d) Power at wind

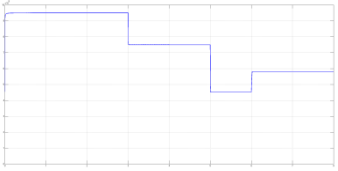

(e) Power at the PV

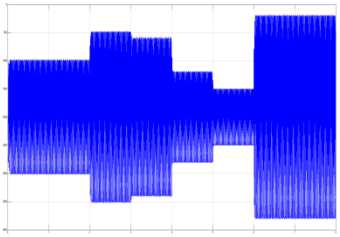

(f) Current at the grid

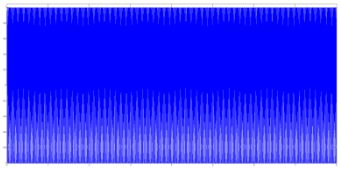

(g) Voltage at the PCC

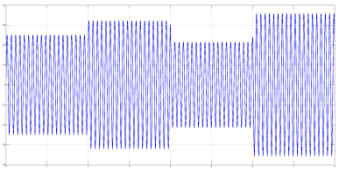

(h) Modulation of VSR

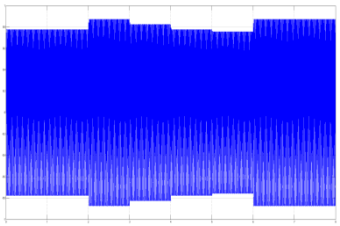

(i) Modulation of VSI

Fig.7 Wind and solar power plant output

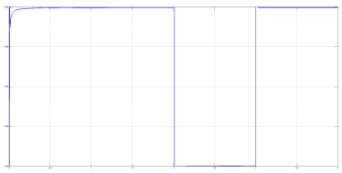

(a) Voltage at the DC-link

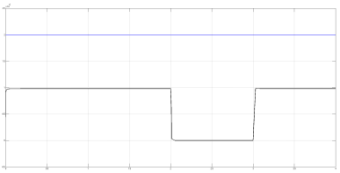

(b) Generated powers of the wind and solar

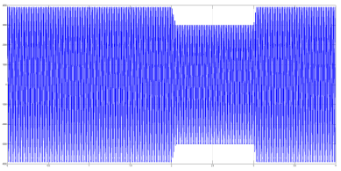

(c) Grid injected current

Fig.8 Only the wind generator's performance

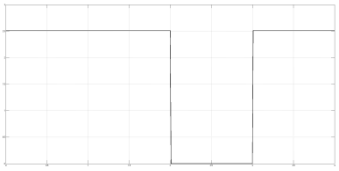

(a) Speed of the PMSG

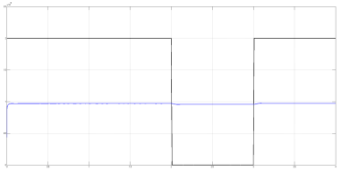

(b) Generated powers of the wind and solar

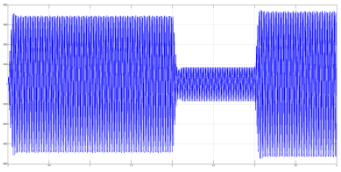

(c) Grid injected current

Fig.9 Only the PV generator's performance

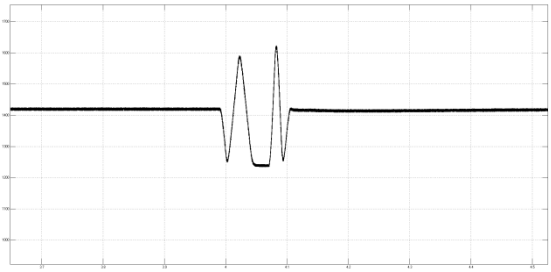

(a)Voltage at the DC-link

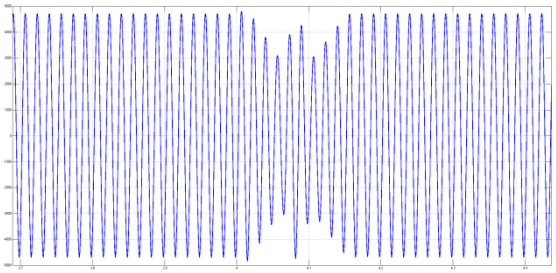

(b) Current at the grid

Fig.10 With deployed fault protection schemes, a response to a 3PG failure occurs in the wind and solar power generation system when the time step is t = 4 seconds and the cycle time step is 4.

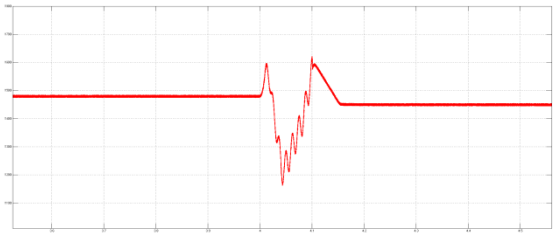

(a) Voltage at the DC-link

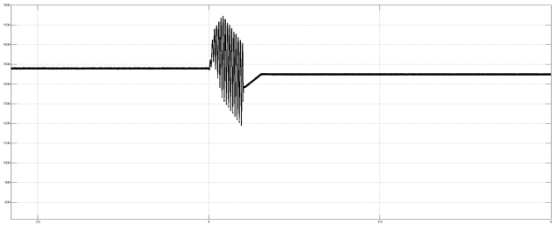

(b) Voltage at the DC-link

Fig. 11 1PG fault at 4:40s, response time of 4 cycles, and 1 P.U. no fault-protection solutions for wind and solar power

RESULTS WITH PROPOSED ANFIS CONTROLLER

Figures 12 and 13 show the combined performance of wind generator and solar generator, whereas figures 14 and 15 show the PV generator's individual performance. Fig. 15 shows the system's performance under 1.0 p.u. wind power generation and solar power generation using the ANFIS controller, when the preceding fault precautions are implemented. Compared to the current PI controller, the dc-link voltage has decreased while the injected ac currents to the grid have remained more stable.

For further research, in Fig. 16, the system's performance under the 1PG fault conditions is examined. Protected in Figure 16, however, the controller's reaction to the DC-link is noticeably smoother than that shown in the preceding controller.

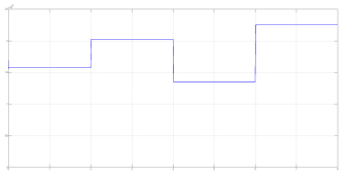

(a) Power at wind

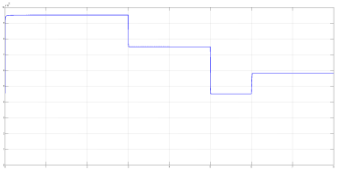

(d)Power at the PV

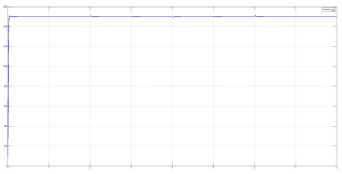

(b) Voltage at the DC-link

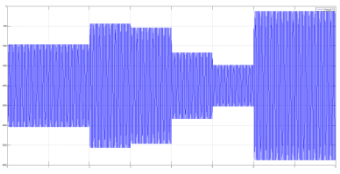

(e) Current at the grid

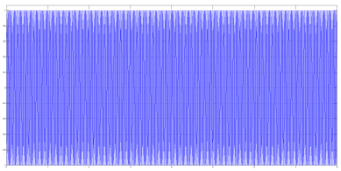

(c) Voltage at the PCC

Fig. 12. Wind and solar power generators Performance

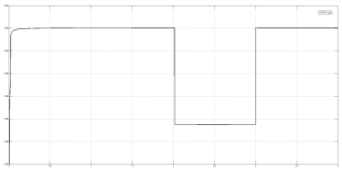

(a)

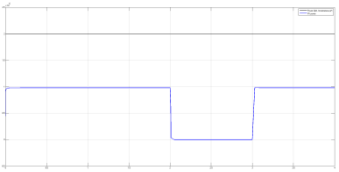

(b)

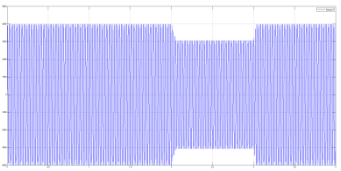

(c)

Fig. 13 Only the wind generator's performance (a) Voltage at the DC-link (b) Generated powers of the wind and solar (c) Grid injected current

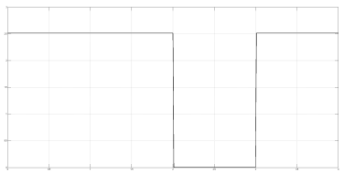

(a)

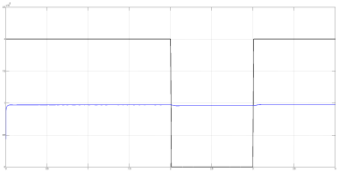

(b)

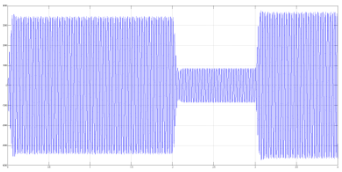

(c)

Fig.14. Only the PV generator's performance (a) Voltage at the DC-link (b) Generated powers of the wind and solar (c) Grid injected current

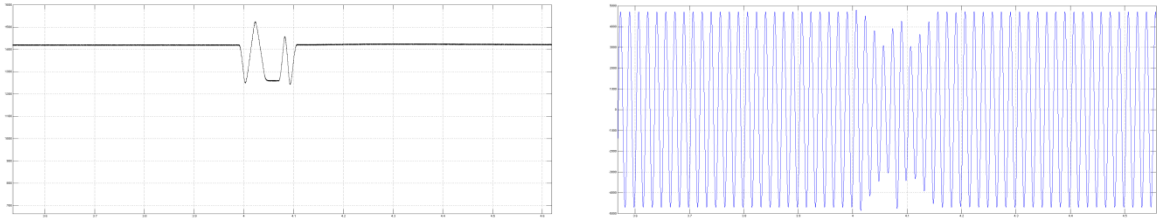

(a)Voltage at the DC-link (b) Current at the grid

Fig. 15. With deployed fault protection schemes, a response to a 3PG failure occurs in the wind and solar power generation system when the time step is t = 4 seconds and the cycle time step is 4.

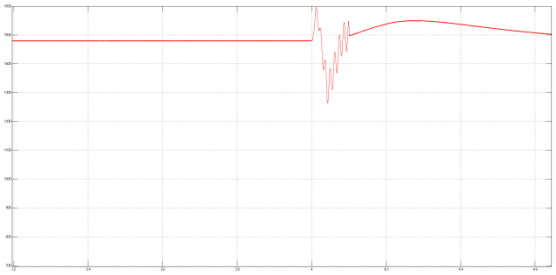

(a)Voltage at the DC-link

Fig. 16. 1PG fault at 4:40s, response time of 4 cycles, and 1 P.U. fault-protection solutions for wind and solar power

CONCLUSION

This research investigates a smart grid based on ANFIS control that is effective at improving power quality. In order to maximise wind power extraction, the voltage source rectifier on the wind generator side is accountable. When it comes to the utility grid, the VSI's primary function is to maximum amount of power extraction from the PV generator, maintain the constant PCC voltage, and balance the input and o/p power across the DC-link capacitor. Network fault tolerance is reduced, and power quality is improved, using the ANFIS control-based technique proposed.

REFERENCES

[1] I. Abdelsalam et.al., "Current source backtoback converter for wind energy conversion systems," IET Renew. Power Gener., vol. 10, no. 10, pp. 1552–1561, 2016.

[2] F. Blaabjerg et.al., "Power electronics as efficient interface in dispersed power generationsystems," IEEE Trans. Power Electron., vol. 19, no. 5, pp. 1184–1194, Sep. 2004.

[3] J. Carrasco et al., "Powerelectronic systems for the grid integration of renewable energy sources—a survey," IEEE Trans. Ind. Electron., vol. 53, no. 4, pp. 1002–1016, Jan. 2006.

[4] A. Yazdani et.al., "A control methodology and characterization of dynamics for a photovoltaicsystem interfaced with a distribution network," IEEE Trans. Power Del., vol. 24, no. 3, pp. 1538–1551, Jul. 2009

[5] L. Nousiainen et al., "Photovoltaic generator as an input source for powerelectronic converters," IEEE Trans. Power Electron., vol. 28, no. 6, pp. 3028–3038, Jun. 2013.

[6] N. Strachan et.al., "Stability of a variable-speed permanent magnet windgenerator with weak ac grids," IEEE Trans. Power Del., vol. 25, no. 4, pp. 2279–2788, Oct. 2010.

[7] P. Mitra et.al., "Offshore wind integration to a weak grid by VSC-HVDC links using power-synchronizationcontrol— A case study," IEEE Trans. Power Del., vol. 29, no. 1, pp. 453–461, Feb. 2014.

[8] Y. Wang et.al., “Control of PMSGbased windturbines for system inertial response and power oscillation damping,” IEEE Trans. Sustain. Energy, vol. 6, no. 2, pp. 565–574, Apr. 2015.

[9] F. Giraud, “Analysis of a utility-interactive wind-photovoltaic hybridsystem with battery storage using neural network,” Ph.D. dissertation, Dept. Electr. Eng., Univ. Massachusetts Lowell, Lowell, MA, USA , 1999.

[10] L. Xu et.al., “An improved optimal sizing method for wind-solar-battery hybrid power system,” IEEE Trans. Sustain. Energy, vol. 4, no. 3, pp. 774–785, Jul. 2013.

[11] S. Sarkar et.al., “MW resource assessment model for a hybrid energy conversion system with wind-solar resources,” IEEE Trans. Sustain. Energy, vol. 2, no. 4, pp. 383–391, Oct. 2011.

[12] Y.-M. Chen et.al., “Multi-input inverter for gridconnected hybrid PVwind power system,” IEEE Trans. Power Electron., vol. 22, no. 3, pp. 1070–1077, May 2007.

[13] S. Bae et.al., “Dynamic modeling and operation strategy for microgrid with windphotovoltaic resources,” IEEE Trans. Smart Grid, vol. 3, no. 4, pp. 1867–1876, Dec. 2012.

[14] B. Mangu et.al., “Grid-connected PVwindbattery based multi-input transformer-coupled bidirectional dc-dc converter for household applications,” IEEE Trans. Emerg. Sel. Topics Power Electron., vol. 4, no. 3, pp. 1086–1095, Sep. 2016.

[15] P. Shanthi et.al., “Effective power transfer scheme for a grid connected hybridwindphotovoltaic system,” IET Renew. Power Gener., vol. 11, no. 7, pp. 1005–1017, 2017.